Manuscript No. BM-D-18-00179 *Rev. 2* *Original*

Unique behavior of dermal cells from regenerative mammal, the African Spiny Mouse, in response to substrate stiffness

Daniel C. Stewart[a], P. Nicole Serrano[b], Andrés Rubiano[c], Ryosuke Yokosawa[c], Justin Sandler[c], Marah Mukhtar[d], Jason O. Brant[b], Malcolm Maden[b], and Chelsey S. Simmons[a,c,e]

[a]J. Crayton Pruitt Family Department of Biomedical Engineering, Herbert Wertheim College of Engineering, University of Florida, PO Box 116131, Gainesville, FL 32611-6131, USA

[b]Department of Biology, College of Liberal Arts and Sciences, University of Florida, PO Box 118525, Gainesville, FL 32611-8525, USA

[c]Department of Mechanical and Aerospace Engineering, Herbert Wertheim College of Engineering, University of Florida, PO Box 116250, Gainesville, FL 32611-6250, USA

[d]Department of Materials Science and Engineering, Herbert Wertheim College of Engineering, University of Florida, PO Box 116250, Gainesville, FL 32611-6250, USA

[e]Division of Cardiovascular Medicine, Department of Medicine, College of Medicine, University of Florida, 1600 SW Archer Road, Gainesville, FL 32610-0277, USA

CORRESPONDING AUTHOR:

Chelsey Simmons
PO Box 116250
Gainesville, FL 32611-6250
Phone: (352) 392-4365
Fax: (352) 392-7303
Email: css@ufl.edu

KEYWORDS: Mechanobiology, wound healing, *Acomys*, dermal fibroblast, keratinocyte

WORD COUNT: 1999

ABSTRACT

The African Spiny Mouse (*Acomys* spp.) is a unique outbred mammal capable of full, scar-free skin regeneration. *In vivo*, we have observed rapid reepithelialization and deposition of normal dermis in *Acomys* after wounding. *Acomys* skin also has a lower modulus and lower elastic energy storage than normal lab mice, *Mus musculus.* To see if the different *in vivo* mechanical microenvironments retained an effect on dermal cells and contributed to regenerative behavior, we examined isolated keratinocytes in response to physical wounding and fibroblasts in response to varying substrate stiffness. Classic mechanobiology paradigms suggest stiffer substrates will promote myofibroblast activation, but we do not see this in *Acomys* DFs. Though *Mus* DFs increase organization of α-smooth muscle actin (αSMA)-positive stress fibers as substrate stiffness increases, *Acomys* DFs assemble very few αSMA-positive stress fibers upon changes in substrate stiffness. *Acomys* DFs generate lower traction forces than *Mus* DFs on pliable surfaces, and *Acomys* DFs produce and modify matrix proteins differently than *Mus* in 2D and 3D culture systems. In contrast to *Acomys* DFs "relaxed" behavior, we found that freshly isolated *Acomys* keratinocytes retain the ability to close wounds faster than *Mus* in an *in vitro* scratch assay. Taken together, these preliminary observations suggest that *Acomys* dermal cells retain unique biophysical properties *in vitro* that may reflect their altered *in vivo* mechanical microenvironment and may promote scar-free wound healing.

1. INTRODUCTION

The African Spiny Mouse (*Acomys* spp.) is a mammal with remarkable regenerative abilities. Following full-thickness skin removal, *Acomys* regenerates in a scar-free manner and replaces dermis, hairs, smooth muscle of the erector pili muscles, sebaceous glands, skeletal muscle of the panniculus carnosus, and adipose cells (Brant et al., 2015; 2016; Seifert et al., 2012). *Acomys* can also regenerate cartilage after an ear punch (Gawriluk et al., 2016; Seifert et al., 2012) and restore cardiac function after myocardial infarction (Qi et al., 2017; 2016). To translate this great potential for regeneration to other mammals, the cellular and molecular basis of *Acomys* scar-free healing must be established.

We previously characterized events of skin regeneration *in vivo* and identified several differences between regenerating *Acomys* and scarring *Mus* skin. Notably, full-thickness *Acomys* skin has a 20x lower modulus and 70x lower toughness than *Mus* skin (Seifert et al., 2012). Since hard surfaces are known to promote myofibroblast activity (Hinz, 2010), we hypothesized that *Acomys* cells isolated from softer microenvironments may maintain an inactivated fibroblast phenotype more readily than *Mus* cells isolated from rigid microenvironments. We were also interested in keratinocytes since stiffer environments often accelerate migration but, conversely, rapid reepithelialization of *in vivo* wounds has been observed in *Acomys*. Here, we have analyzed epidermal keratinocytes and dermal fibroblasts from *Acomys* and *Mus* to determine functional differences between the two cell types that may contribute to dermal wound healing.

2. MATERIALS AND METHODS

2.1 Isolation and culture of primary cells. Protocols and care of *Acomys cahirinus* (University of Florida colony) and outbred CD-1 *Mus musculus* (Charles River) were approved

by UF Institutional Animal Care and Use Committee and were within US animal welfare regulations and guidelines.

Cells that had gone through less than 3 population doublings after isolation from newborn pups of *Acomys* (5-week gestation) and *Mus* (3-week gestation) were used for these experiments. Birth is well beyond the stage when embryos can heal without scarring *in utero* (embryonic day 16.5 in *Mus*), thus fibroblasts were obtained from "scarring" stages. Pups were euthanized and the dorsal skin removed. Dermis and epidermis were separated after overnight incubation at 4°C in 0.125% Trypsin with EDTA (Gibco). The dermis was further incubated in 0.1% collagenase type-1 (Gibco) for 1.5 hrs at 37°C to separate cells and then washed and cultured in DMEM with 10% FBS, 10% NuSerum (Corning), 0.1% insulin-transferrin-selenium, and 0.1% penicillin/streptomycin. The epidermis was triturated and filtered, and isolated cells were cultured in keratinocyte-specific medium (Lifeline® DermaK) supplemented with pen/strep.

2.2. *In vitro* wound healing assay. Primary keratinocytes were seeded at $2x10^5$ cells per well in 24-well plates overnight. Cell layer was scratched using a sterile pipette tip and imaged directly after scratching. Images of the same scratched region were taken with phase contrast every three hours. The rate of closure was calculated using ImageJ (NIH).

2.3. Silicone substrate fabrication. Polydimethylsiloxane (PDMS, Sylgard527 and Sylgard184, Dow Corning) was mixed per manufacturer's instructions, poured into a tissue culture plate, degassed, and cured at 50°C. Surfaces were plasma treated (PDC-001-HP, Harrick) for 25 s and submerged in deionized water (DIW). Samples were rinsed, covered with sterile DIW, and sterilized by germicidal UV. PDMS and plastic dishes were coated with 10 μg/mL rat-tail collagen I (ColI, Corning) solution.

2.4 Immunofluorescence and Western Blot. *Acomys* and *Mus* dermal fibroblasts (DFs) were plated onto PDMS and plastic surfaces at 5,000 cells/cm^2 in normal serum-containing medium for 48 hours. To preserve the F-actin/αSMA structure, cells were treated with 3% paraformaldehyde (PFA) and 0.01% Triton-X100 for 5 min, further fixed for 10 min in 3% PFA, and blocked in 1% BSA for 30 min. Cells were then labeled for F-actin (Phalloidin-FITC, 1:150 in 1% BSA, Sigma) for 40 min and αSMA (αSMA-Cy3 monoclonal antibody,1:200 in 1% BSA, Sigma#C6198) for 1 hr. Analyzing our preliminary *Acomys* genome assembly, αSMA shows 99.4% identity with *Mus* αSMA. Additionally, the antibody used cross-reacts with 12 animals including canines, humans, frogs, and mice. Images were acquired (Nikon Ni-Eclipse) with a 40x immersion objective. All images were taken at identical settings for comparison and subsequent quantification in MATLAB R2016a (Mathworks). Statistics were performed in JMP Pro 13 (SAS).

For Western Blot, cell extracts from DFs on plastic were made with RIPA buffer, and equal amounts of protein were loaded onto a 4-12% bis-tris gel and blotted onto a PVDF membrane. αSMA antibody (Abcam#5694) with high-species cross-reactivity was used. The membrane was incubated with 1:10,000 dilution of αSMA antibody or GAPDH made up in 5% BSA in TBST overnight, then with an HRP secondary antibody at 1:1000. Bands were visualized with a chemiluminescence kit and imaged on a FluorChem imager.

To visualize ECM production, primary DFs were seeded at 15x10^4 in untreated 24-well plates, grown to confluency, washed with PBS, fixed for 30 minutes in 4% PFA, permeabilized with 0.1% TX-100, and blocked with 0.5% BSA. Individual wells were incubated with ColI, ColIII, or ColIV primary antibodies (1:100; Abcam) followed with AlexaFlour488-conjugated anti-rabbit or anti-mouse IgG (1:500; Abcam) and imaged using Olympus IX81 40X-objective.

2.5. Traction Force Microscopy (TFM). Two-layered polyacrylamide (PA) hydrogel substrates (E~50 kPa) were fabricated for TFM as in Simmons et al. (Simmons et al., 2013). Gel surface was SulfoSANPAH functionalized, sterilized by germicidal UV, and coated with 100 μg/mL ColI for 30 minutes before seeding 10,000 cells per substrate. Cells were allowed to attach for 18-24 hours before transfer to a temperature-controlled stage (Nikon Ti-E). One brightfield image of the attached cell was acquired with a fluorescence image of beads. Cell locations were stored (Nikon Elements) then cells removed using trypsin, and second image of "null" beads acquired. Calculations of bead displacements (PIVLab (Thielicke and Stamhuis, 2014)) and strain energy (Fourier-transform traction cytometry (Sabass et al., 2008)) were done in MATLAB. Area and roundness were quantified by manually outlining cell border and running "Measure" in ImageJ, where roundness = $\frac{4 \cdot Area}{\pi \cdot Major\ Axis^2}$. Wilcoxon non-parametric tests were used to compare calculated strain energy (one-sided test) and cell area and roundness (two-sided test) in JMP Pro 13.

To demonstrate fidelity of mechanism for cell-generated traction forces, *Mus* and *Acomys* DFs were plated on ColI-coated compliant PDMS substrates (E~5kPa compared to E~50 kPa for PA hydrogels). After 24 hours in serum-containing medium, two brightfield images (2.31 mm^2) from two wells of each species were taken. Wrinkling was assessed by thresholding images and counting pixels in ImageJ.

2.6. Cell-Embedded Collagen Hydrogels. High concentration ColI is diluted with 0.2% acetic acid and combined in a 3:1 ratio with 5x DMEM (Sigma), 1M HEPES (Gibco), and DFs to fabricate 3mg/mL collagen hydrogels with 2,000 cells per 55 μL gel. Precursor solution is maintained at 4°C and then incubated at 37°C for 30 minutes. Constructs are then hydrated with media and kept in 37°C CO_2 incubator. Gels were fixed with 4% PFA in PBS and later

lyophilized using a critical point drier (Tousimis, autosamdri-815). Samples were coated with carbon using a sputter coater (Denton DeskV) and imaged with a Scanning Electron Microscope (Hitachi SU5000).

3. RESULTS AND DISCUSSION

3.1. *Acomys cahirinus* keratinocytes close *in vitro* wounds faster than *Mus musculus.*

In vivo, *Acomys* appear to reepithelialize wounds more quickly than *Mus*, but scabs can obscure visualization of epithelial migration and calculation of wound closure rates. *In vitro*, wound healing rates were more than twice as fast for *Acomys* keratinocytes (AKs, 0.021 mm^2/hour) than *Mus* keratinocytes (MK, 0.009 mm^2/hour). AKs closed scratches under 30 hours whereas most MK scratches were still detectable 48 hours later (Fig. 1). This *in vitro* migration behavior is consistent with *in vivo* observations (Seifert et al., 2012).

3.2. αSMA expression in *Acomys* dermal fibroblasts does not change with substrate stiffness.

During wound healing, fibroblasts become activated myofibroblasts that produce inflammatory factors and assemble dense extracellular matrix (ECM). One sign of myofibroblast activation is increased αSMA expression as fibroblasts generate higher contractile forces to close wounds (Hinz, 2010), and such αSMA expression has been induced *in vitro* by culturing fibroblasts on substrates with hyper-physiological stiffness (Achterberg et al., 2014; Goffin et al., 2006; Quinlan and Billiar, 2012; Scott et al., 2017; Wang et al., 2013). Since *Acomys* does not have activated myofibroblasts *in vivo* after wounding and *Acomys* skin is softer than *Mus* (Seifert et al., 2012), we hypothesized that *Acomys* DFs would not assemble αSMA-positive stress fibers in response to stiff substrates.

We did observe less αSMA assembly in *Acomys* fibroblasts (ADFs) than *Mus* fibroblasts (MDFs) on substrates of increasing stiffness. MDFs had clear, organized αSMA-positive fibers

that increased proportionally with substrate stiffness (Fig. 2A), similar to previous findings (Achterberg et al., 2014; Goffin et al., 2006). In contrast, we saw no significant difference in αSMA localization in ADFs between substrates (Fig. 2A,D-E). Quantification of αSMA and F-actin fluorescence showed that ADFs had lower αSMA values compared to MDFs that remained constant across stiffnesses, and we confirmed by Western blot that ADFs on plastic produce αSMA (Fig. 2C). Both DFs assembled F-actin fibers, though F-actin fibers were more pronounced in MDFs (Fig. 2B). These data suggest that ADFs cannot be activated into myofibroblasts by stiff substrates alone. Since *Acomys* gestation takes longer than *Mus, Acomys* newborn fibroblasts are actually "older" than *Mus*, which accentuates this surprising response of ADFs.

3.3. *Acomys* fibroblasts generate lower contractile forces than *Mus* fibroblasts. Since αSMA enhances but is not required for contractile force generation (Chen et al., 2007), we sought to quantify ADF and MDF traction forces and hypothesized that ADFs would generate lower cellular traction forces than MDFs. ADFs did generate lower traction forces than MDFs on PA substrates (1.0 ± 0.6 pJ versus 2.4 ± 1.8 pJ, $p = 0.04$, $n = 12$ each). Median ± median absolute deviation reported to reflect non-parametric statistical analysis. Cell spread area and roundness were similar between cell populations (Fig. 3B-C), so calculated differences likely reflect true differences in contractility and not cell shape. To examine differences in traction force on different substrates, wrinkle analysis on ~5 kPa silicone confirmed greater contractility in *Mus* (Fig. 3F-3H) compared to *Acomys*.

In normal mammalian fibroblasts, contractility is required for many processes central to fibrosis, including migration (Case and Waterman, 2015; Shi-wen et al., 2009), matrix protein production (Mun et al., 2014), and activation of TGFβ, a pro-fibrotic cytokine (Mun et al., 2014;

Wipff et al., 2007). Matrix stiffness has been shown to promote these fibrotic processes *in vitro,* suggesting lack of response to stiff substrates in *Acomys* may contribute to *Acomys* regeneration though exact mechanisms remain to be identified.

3.4. *Acomys* fibroblasts produce less matrix in 2D and 3D environments. In addition to increased αSMA expression and contractility, activated myofibroblasts produce and crosslink excess collagen. We then asked whether there were differences in fibroblast production of ECM proteins. Both MDFs and ADFs expressed ColI but with a greater intensity in MDFs (Fig. 4A-B). Only MDFs expressed ColIII (Fig. 4C-D) and both cell types expressed ColIV (Fig. 4E-F). These results are somewhat surprising since ColIII is thought to be a regenerative collagen (Volk et al., 2011).

We also observed fibroblast remodeling in 3D. MDFs encapsulated in collagen spread and increase matrix stiffness over 7 days in culture (Figure 4G,I), as expected from normal mammalian fibroblasts (see example review (Brown, 2013)). ADFs, on the other hand, do not spread nor remodel surrounding gel (Figure 4H,J). When characterized by indentation after 7 days in culture, the MDF-embedded matrix was stiffer than the *ADF*-embedded matrix (1500 and 800 Pa, respectively).

4. CONCLUSION

The data presented here confirm the unique behavior of *Acomys* keratinocytes and DFs is conserved *in vitro*. We have shown that *Acomys* keratinocytes migrate faster than *Mus* keratinocytes to close an imposed wound region. We have also demonstrated that *Acomys* DFs do not adapt a myofibroblast phenotype *in vitro* as they fail to assemble αSMA-positive stress fibers in response to increasing substrate stiffness, generate lower contractile forces than their

Mus counterparts, and do not produce excess collagen in 2D nor 3D compared to *Mus* DFs. Collectively, the behavior shown here suggests alterations in ADF mechanosensing pathways and provides the groundwork for extensive future investigations into mechanisms of mammalian regeneration.

ACKNOWLEDGEMENTS

This work was supported by the National Science Foundation (CMMI BMMB 1636007) and the W. M. Keck Foundation. Study sponsors had no role in the study design, experimentation, writing, nor submission of the manuscript.

CONFLICT OF INTEREST STATEMENT

Authors disclose no financial and personal relationships with other people or organizations that could inappropriately bias their work.

REFERENCES

Achterberg, V.F., Buscemi, L., Diekmann, H., Smith-Clerc, J., Schwengler, H., Meister, J.-J., Wenck, H., Gallinat, S., Hinz, B., 2014. The nano-scale mechanical properties of the extracellular matrix regulate dermal fibroblast function. Journal of Investigative Dermatology 134, 1862–1872.

Brant, J.O., Lopez, M.-C., Baker, H.V., Barbazuk, W.B., Maden, M., 2015. A Comparative Analysis of Gene Expression Profiles during Skin Regeneration in Mus and Acomys. PLoS ONE 10, 1-19.

Brant, J.O., Yoon, J.H., Polvadore, T., Barbazuk, W.B., Maden, M., 2016. Cellular events during scar-free skin regeneration in the spiny mouse, Acomys. Wound Repair and Regeneration 24, 75–88.

Brown, R.A., 2013. In the beginning there were soft collagen-cell gels: towards better 3D connective tissue models? Experimental Cell Research 319, 2460–2469.

Case, L.B., Waterman, C.M., 2015. Integration of actin dynamics and cell adhesion by a three-dimensional, mechanosensitive molecular clutch. Nature Cell Biology 17, 955–963.

Chen, J., Li, H., SundarRaj, N., Wang, J.H.-C., 2007. Alpha-smooth muscle actin expression enhances cell traction force. Cytoskeleton 64, 248–257.

Gawriluk, T.R., Simkin, J., Thompson, K.L., Biswas, S.K., Clare-Salzler, Z., Kimani, J.M., Kiama, S.G., Smith, J.J., Ezenwa, V.O., Seifert, A.W., 2016. Comparative analysis of ear-hole closure identifies epimorphic regeneration as a discrete trait in mammals. Nature Communications 7, 11164.

Goffin, J.M., Pittet, P., Csucs, G., Lussi, J.W., Meister, J.-J., Hinz, B., 2006. Focal adhesion size controls tension-dependent recruitment of alpha-smooth muscle actin to stress fibers. Journal of Cell Biology 172, 259–268.

Hinz, B., 2010. The myofibroblast: paradigm for a mechanically active cell. Journal of Biomechanics 43, 146–155.

Mun, J.-H., Kim, Y.-M., Kim, B.-S., Kim, J.-H., Kim, M.-B., Ko, H.-C., 2014. Simvastatin inhibits transforming growth factor-beta1-induced expression of type I collagen, CTGF, and alpha-SMA in keloid fibroblasts. Wound Repair and Regeneration 22, 125–133.

Qi, Y., Goel, R., Mandloi, A.S., Vohra, R., Walter, G., Joshua, Y.F., Gu, T., Katovich, M.J., Aranda, J.M., Maden, M., Raizada, M.K., Pepine, C.J., 2017. Spiny mouse is protected from ischemia induced cardiac injury: leading role of microRNAs. The FASEB Journal 31, S721.4.

Qi, Y., Zhang, J., Wang, L., Kumar, A., Vohra, R., Walter, G.A., Maden, M., Katovich, M.J., Raizada, M., Pepine, C.J., 2016. Intrinsic increased ACE2 expression protects spiny mouse Acomys Cahirinus against ischemic-induced cardiac dysfunction. The FASEB Journal 30, lb561–lb561.

Quinlan, A.M.T., Billiar, K.L., 2012. Investigating the role of substrate stiffness in the persistence of valvular interstitial cell activation. Journal of Biomedical Materials Research Part A 100, 2474–2482.

Rubiano, A., Delitto, D., Han, S., Gerber, M., Galitz, C., Trevino, J., Thomas, R.M., Hughes, S.J., Simmons, C.S., 2018. Viscoelastic properties of human pancreatic tumors and in vitro constructs to mimic mechanical properties. Acta Biomaterialia 67, 331-340.

Sabass, B., Gardel, M., Waterman, C., Schwarz, U., 2008. High resolution traction force microscopy based on experimental and computational advances. Biophysical Journal 94, 207–220.

Scott, R.A., Kharkar, P.M., Kiick, K.L., Akins, R.E., 2017. Aortic adventitial fibroblast sensitivity to mitogen activated protein kinase inhibitors depends on substrate stiffness. Biomaterials 137, 1–10.

Seifert, A.W., Kiama, S.G., Seifert, M.G., Goheen, J.R., Palmer, T.M., Maden, M., 2012. Skin shedding and tissue regeneration in African spiny mice (Acomys). Nature 489, 561–565.

Shi-wen, X., Liu, S., Eastwood, M., Sonnylal, S., Denton, C.P., Abraham, D.J., Leask, A., 2009. Rac Inhibition Reverses the Phenotype of Fibrotic Fibroblasts. PLoS ONE 4, 1–9.

Simmons, C.S., Ribeiro, A.J.S., Pruitt, B.L., 2013. Formation of composite polyacrylamide and silicone substrates for independent control of stiffness and strain. Lab on a Chip 13, 646–649.

Thielicke, W., Stamhuis, E.J., 2014. PIVlab - Towards User-friendly, Affordable and Accurate Digital Particle Image Velocimetry in MATLAB. Journal of Open Research Software 2, 1202–10.

Volk, S.W., Wang, Y., Mauldin, E.A., Liechty, K.W., Adams, S.L., 2011. Diminished type III collagen promotes myofibroblast differentiation and increases scar deposition in cutaneous wound healing. Cells Tissues Organs 194, 25–37.

Wang, H., Tibbitt, M.W., Langer, S.J., Leinwand, L.A., Anseth, K.S., 2013. Hydrogels preserve native phenotypes of valvular fibroblasts through an elasticity-regulated PI3K/AKT pathway. Proceedings of the National Academy of Sciences of the United States of America 110, 19336–19341.

Wipff, P.-J., Rifkin, D.B., Meister, J.-J., Hinz, B., 2007. Myofibroblast contraction activates latent TGF-beta1 from the extracellular matrix. Journal of Cell Biology 179, 1311–1323.

Figure Captions for Manuscript No. BM-D-18-00179, Revision 2, "Unique behavior of dermal cells from regenerative mammal, the African Spiny Mouse, in response to substrate stiffness"

Figure 1: *Acomys cahirinus* keratinocytes (AKs) migrate faster than *Mus musculus* keratinocytes (MKs) during wound closure. (A) Sample images of keratinocyte cultures at 0 hrs and 27 hrs after induced scratch. Scale bars are 200 μm. (B-C) AKs migrated and closed the scratch area within 30 hr while MKs require more than 48 hours to close completely. Bars depict mean ± standard error, $n \geq 8$ for each condition.

Figure 2: Substrate stiffness does not upregulate αSMA expression in *Acomys* dermal fibroblasts (ADFs). (A) *Mus* dermal fibroblasts (MDFs) upregulate αSMA (red) proportionally on silicone substrates with increasing stiffness (top row), while ADFs did not show any significant changes in αSMA expression (bottom row). Both cell types assemble F-actin fibers (green), though MDFs assemble more vivid, discrete fibers on higher stiffness substrates. Scale bars are 25 μm. (B) Quantification of F-actin-positive pixels normalized to number of nuclei confirms ADFs spread and form an F-actin cytoskeleton, but no significant increase is seen in ADFs in response to stiffness compared to MDFs ($n = 46$ for *Acomys*, $n = 53$ for *Mus*). Bars depict median ± median absolute deviation. (C) Western blot confirms αSMA (42 kDa) is produced by ADFs on plastic and recognized by commercial antibodies. Equal amounts of protein including GAPDH 37 kDa control were run in each lane for both species on a single gel. Molecular weight standards (kDa) shown in left column. (D) Quantified pixel count of αSMA-positive pixels normalized to number of nuclei shows ADFs (blue data points) do not assemble as much αSMA as MDFs (orange data points) in response to stiffness. No significant difference is seen in αSMA production per nuclei between ADFs on different stiffnesses, while MDFs had significantly more αSMA with increasing stiffness compared to ADFs. Bars depict median ± median absolute deviation. (E) ADFs do not have significant fold-change between stiffnesses while MDFs have 1.5x increase (Sylgard 184, E ~ 1 MPa) and 3x increase (TCP, E ~ 3 GPa) in αSMA as substrate stiffness increases. Fold-change was determined by normalizing to the average number of αSMA-positive pixels on Sylgard 527 (E ~ 5 kPa). No significant difference was seen between ADFs on all stiffnesses or MDFs on Sylgard 527. Bars depict mean ± standard error. Statistics were determined using a Wilcoxon non-parametric multiple comparison test. *$p<0.03$, **$p<0.0001$

Figure 3: *Acomys* dermal fibroblasts (ADFs) generate less traction energy than *Mus* dermal fibroblasts (MDFs) while having similar cell morphologies. (A) Strain energy represents work done per cell, and ADFs generated significantly less strain energy on polyacrylamide hydrogel surfaces than MDFs ($p = 0.04$). (B-C) Cells from both species had similar cell area and roundness. Black bars depict the median. (D-E) Traction stresses of representative ADFs and MDFs. (F-G) On complaint silicone substrates (~5 kPa), MDFs generate enough force to wrinkle

surface while ADFs do not. (H) Quantification of wrinkling (bright white areas) confirms MDFs deform the surface more than ADFs (n = 4 independent regions (2.31 mm^2) per species). Bars depict mean ± standard error. All scale bars are 50 μm.

Figure 4: *Acomys* dermal fibroblasts (ADFs) produce less matrix *in vitro* than *Mus* dermal fibroblasts (MDFs). ADFs and MDFs expressed collagen I (*Col I*, A,B) and collagen IV (*Col IV*, E,F) at similar levels, but MDFs expressed more collagen III (*Col III*) than ADFs (C,D). In 3D collagen I gels, MDFs are more stellate than spheroidal ADFs (G,H). Day 7 remodeled matrix of gels embedded with MDFs (I) are twice as stiff as those embedded with ADFs (J). Modulus values are nominal average of 3 indentations on 3 gels each (n = 9) using protocols from Rubiano et al. (Rubiano et al., 2018). All scale bars are 10 μm.

Figure 1
Click here to download high resolution image

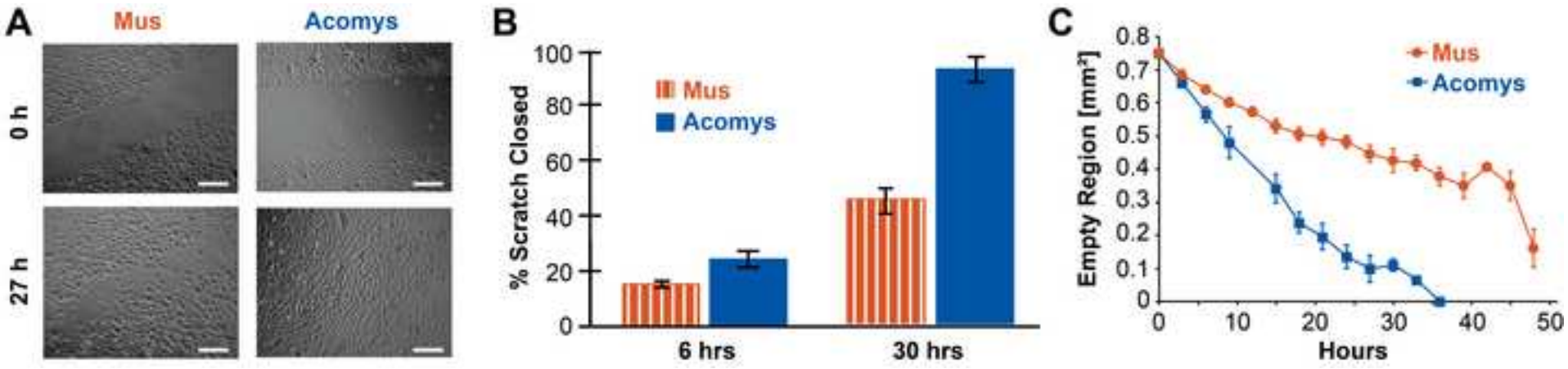

Revised Figure 2

Click here to download high resolution image

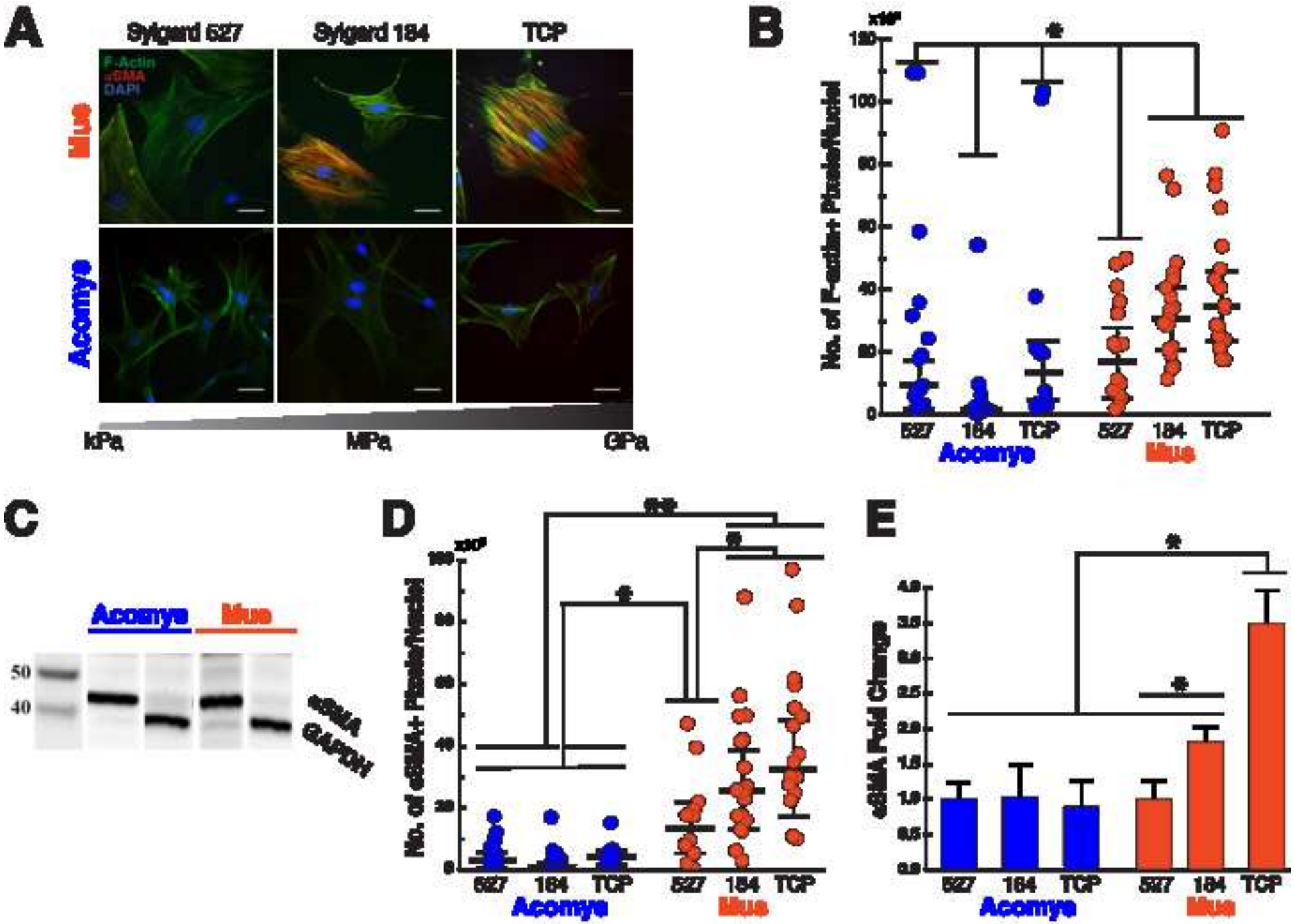

Revised Figure 3

Click here to download high resolution image

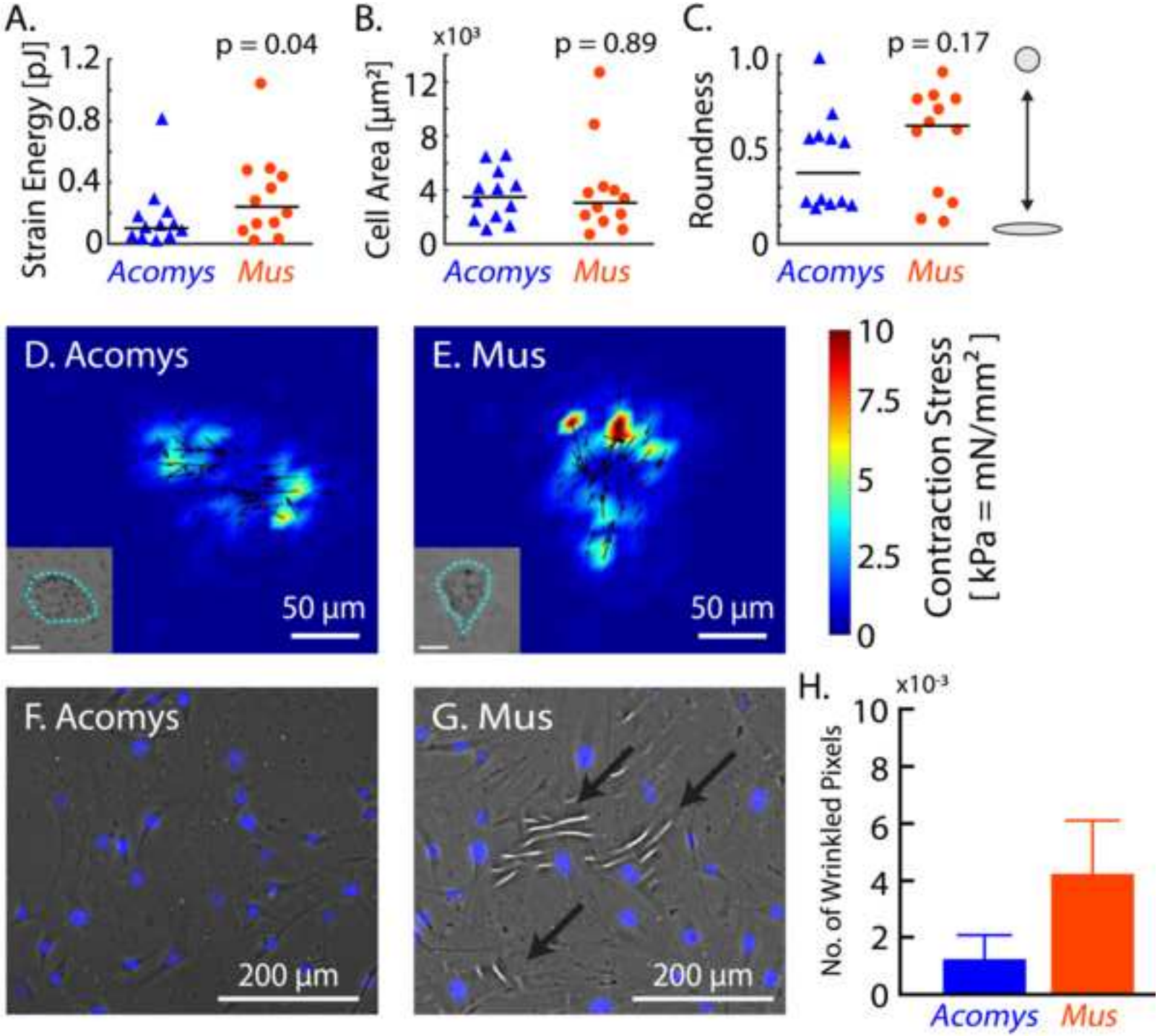

Figure 4

Click here to download high resolution image